Gradients of potential fields on rough surfaces: Perturbative calculation of the singularity distribution function $f(\alpha)$ for small surface dimension

Kausik Sarkar and Charles Meneveau
Department of Mechanical Engineering, Johns Hopkins University, Baltimore, Maryland 21218
(Received 30 September 1992)

An exact solution to the Laplace equation with Dirichlet boundary conditions on a simple boundary is used in an iterative fashion to study the case of a *stochastic* rough surface with fractal dimension $D=2+\epsilon$. For small ϵ, an analytic expression is derived for the spectrum of singularities $f(\alpha)$ of the gradient of the potential normal to the boundary, using the random multiplier approach. A binomial approximation to the multiplicative process is shown to severely underestimate $f(\alpha)$ for low values of α.

PACS number(s): 02.50.−r, 44.10.+i

I. INTRODUCTION

Many problems of physical interest involve fields satisfying Laplace's equation with Dirichlet boundary conditions. Examples include conduction (or diffusion) from a surface at a fixed temperature (or concentration), potential flow of an ideal fluid over a body, electric field around a charged object, etc. For domains bounded by surfaces that are differentiable almost everywhere, a variety of methods to solve Laplace's equation exist. Motivating the work reported here are the problems of diffusion, conduction, etc., involving a rough boundary. Such surfaces may appear, down to a certain spatial resolution, to be nondifferentiable everywhere and/or may exhibit convolutions over many length scales. Random fractals can be used as a first-order model for such rough surfaces. Their apparent complexity is the result of simple rules that are applied repeatedly at different length scales, and they can be (partially) characterized by their fractal dimension D. Many material surfaces have been reported to exhibit fractal (geometrically self-similar) behavior and their dimensions D have been measured.

On the other hand, Laplace's equation with moving Dirichlet boundary condition governs diffusion-limited-aggregation processes (DLA). This has been suggested as a model for various natural phenomena as diverse as dielectric breakdown and viscous fingering since it was first proposed by Witten and Sanders [1]. Computer simulations and experiments (see, e.g., Feder [2] and Pietronero and Wiesmann [3]) have shown its fractal dimension to be ~ 1.7 (in two dimensions) and ~ 2.5 (in three dimensions). The shape of fractal growth patterns were studied analytically by renormalization-group theory [4–6], by fixed-scale transformation [7], and by numerical simulations [8]. The results of numerical simulations also suggested multifractal behavior of the growth velocity at different points of the cluster [9]. This velocity is equal to the gradient of the Laplacian field normal to the boundary, called (once normalized) the "harmonic measure." Multifractal behavior refers to the highly intermittent and self-similar structure of this gradient, caused by the "screening" of the field by the boundary itself.

In turbulent shear flows, irrotational (potential) velocity fluctuations occur outside the turbulent interface. Such surfaces have been shown to possess fractal scaling [10] and their dimension (typically $\sim\frac{7}{3}$) has been measured. These are highly unsteady surfaces, where the boundary condition for the potential flow problem needs to be prescribed [11,12]. To lay proper ground for future work on this problem, it is useful for now to consider the simpler case of a stationary boundary of fractal dimension D with Dirichlet boundary condition. A considerable amount of work exists in this area for deterministic fractal boundaries, and many interesting results are available in the mathematics literature [13–17]. The latter concentrates on upper bounds for the dimension of the harmonic measure in two- and three-dimensional domains. Using a more empirical approach, Everstz and Mandelbrot [18] obtain a numerical solution to the Laplace equation around an exactly self-similar Koch tree in two dimensions. Their logarithmic rendering of the calculated potential levels around successive prefractals illustrates the multiplicative nature of the Laplacian potential, and hence of the harmonic measure. Progressive refinement of the boundary and the measure supported on it is used to establish an intuitive connection between the multifractality of the measure and the underlying multiplicative process.

In the present study, we construct a self-similar random surface, embedded in a three-dimensional domain. The surface is generated by randomly distributing bumps (hemispheres) of progressively smaller sizes. Arguably, such random fractals are more realistic for modeling rough surfaces than their deterministic counterparts. The goal of the present study then is to statistically characterize the gradient of the potential field on this boundary as completely as possible. Laplace's equation is solved perturbatively. Numerical results of Everstz and Mandelbrot [18] suggested the perturbative method, for they found numerically that the successive addition of geometric details affect the larger-scale solution attained around earlier generations very little. The procedure is based on the *analytic* solution of Laplace's equation for a single isolated bump placed on an otherwise infinite plane with a constant flux from the plane. Smaller bumps are assumed to add a small-scale perturbation on the larger-scale solution, and the mutual effect between the bumps of the same generation is neglected. This becomes exact

 ©1993 The American Physical Society

in the limit of sparse distribution of bumps and large difference in size of successive bumps.

In Sec. II, the mathematical formulation of the boundary-value problem is detailed. Section III presents a hierarchical generation procedure for the fractal surface. It has two parameters, radius ratio b and covered area fraction ρ, and when continued indefinitely this generates a fractal surface of dimension D. In Sec. IV, the perturbative procedure is presented, and a multiplicative solution is obtained. In Sec. V, the multifractal formalism is used to describe the resulting statistics. This is done using the random multiplier approach. In Sec. VI, a binomial approximation to the multiplicative process is attempted and the results are compared to those of the random multiplier approach. Section VII summarizes the results and explores the implications on the properties of the potential field at various distances from the boundary.

II. MATHEMATICAL FORMULATION

Laplace's equation will be solved in three dimensions, with a homogeneous Dirichlet boundary condition on a fractal surface, which forms the lower boundary of the domain. This lower boundary is assumed to have infinite extent in the horizontal direction. The other boundary is sufficiently far above this surface. The boundary condition there is such as to create an overall average flux density Λ on the surface. The pertinent mathematical system is

$$\nabla^2\phi=0 \ , \quad \text{in } \Omega \ , \tag{1}$$

$$\phi=0 \ , \quad \text{on } \partial\Omega_l \ , \quad \frac{\partial\phi}{\partial z}=\Lambda \ , \quad \text{as } z\to\infty \ , \tag{2}$$

where $\partial\Omega_l$ is the lower boundary and z is the vertical coordinate.

III. SURFACE CHARACTERIZATION

In this section, the lower boundary is described and its fractal dimension derived. In order to generate a fractal surface with a minimal stochastic characterization, a step by step hierarchical generation process with a few geometric parameters is adopted. For definiteness, we start with a portion of an initial smooth area S. On the plane, hemispherical 1-bumps (first generation) of certain radius a_1 are placed with number density c_1 per unit area (of the plane). The area fraction covered by 1-bumps is $\rho_1=c_1(\pi a_1^2)$ and the area fraction of the remaining part of the plane is $\omega_1=(1-\rho_1)$. In general ρ_i,ω_i denote the corresponding extension for ith stage of the prefractal surface. The total areas of the 1-bumps $\{1\}$ and the remainder plane $\{0\}$ are, respectively,

$$2\rho_1 S, \quad \omega_1 S \ . \tag{3}$$

Next, on this first generation surface second generation bumps (2-bumps) of radius a_2 are placed with the same number density c_2 both on the remaining plane and on the 1-bumps. There are now four distinct types of sites on this prefractal, 2-bumps on 1-bumps $\{11\}$, 1-bumps on the plane $\{01\}$ (or "plane " on 1-bumps), and 2-bumps on plane $\{10\}$, and plane $\{00\}$. The total areas of these four types of sites are, respectively,

$$2^2\rho_2\rho_1 S \ , \quad 2\omega_2\rho_1 S \ , \quad 2\rho_2\omega_1 S \ , \quad \omega_2\omega_1 S \ . \tag{4}$$

The process is then continued ideally *ad infinitum*. In order to generate a fractal surface, geometric self-similarity is enforced through two conditions. The covered area fraction is fixed, i.e., $\rho_i=\rho_{i+1}\equiv\rho$, which results in

$$\frac{c_i}{c_{i+1}}=\frac{a_{i+1}^2}{a_i^2} \ . \tag{5}$$

The second condition is that the ratio of successive radii is fixed as

$$b\equiv\frac{a_{i+1}}{a_i}=\left[\frac{c_i}{c_{i+1}}\right]^{1/2} \ . \tag{6}$$

This prescription is consistent with the assumed self-similarity of the fractal surface and is illustrated in Fig. 1. With these assumptions, sites like $\{01\}$ and $\{10\}$ in (4) have the same surface area. Similarly, for higher generations, the sites with the same number of 1's in their binary representation are identified. After n iterations, a very uneven surface with the following statistics of area fractions for the different sites is obtained:

Binary representation	Total area	Number
$\{1111\ldots n$ 1's$\}$	$S(2\rho)^n$	${}^nC_0$
$\vdots$	$\vdots$	$\vdots$
$\{0111\ldots k$ 1's, $(n-k)$0's$\}$	$S(2\rho)^k(1-\rho)^{n-k}$	${}^nC_k$
$\vdots$	$\vdots$	$\vdots$
$\{0000\ldots n$ 0's$\}$	$S(1-\rho)^n$	${}^nC_n$,

where ${}^nC_k=n!/[k!(n-k)!]$. The nth generation has a total area of

$$A=S\sum_{k=0}^{n}{}^nC_k(2\rho)^k(1-\rho)^{n-k}=S(1+\rho)^n \ . \tag{7}$$

In terms of the smallest relevant length scale $a_n=a_0b^n$ (radius of the n-bumps), this can be written (for large n) as

$$S(1+\rho)^n\sim S\left[\frac{a_n}{a_0}\right]^{2-D} \ , \tag{8}$$

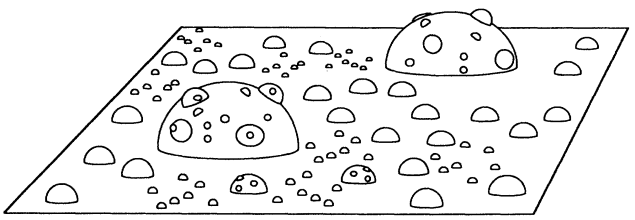

FIG. 1. Sketch of a fractal surface generated by semihemispherical bumps placed on an initially smooth plane. Shown is a prefractal after two stages of the construction process.

where

$$D=2-\log_b(1+\rho) \tag{9}$$

is the fractal dimension of the surface. The surface with fractal dimension D is generated with two free parameters b and ρ. It is to be noted that at any generation, the exact locations of the bumps with reference to the previous generation configuration are not specified, except for the assumption that they do not overlap. This is more in conformity with the spirit of the randomness encountered in real surfaces and is in contrast to the construction of fully deterministic fractals (e.g., the Koch curve). Also it is evident from (9) that for a particular D a range of fractal surfaces can be obtained for different pairs of b and ρ. As will be seen in Sec. V several constraints need to be placed on b and ρ.

IV. PERTURBATIVE SOLUTION OF THE LAPLACE EQUATION

The elementary building block of the proposed procedure is the solution due to a hemispherical bump on an otherwise infinite plane. In the absence of the bump, we find the zeroth-order solution

$$\phi^{(0)}=\Lambda z \ , \tag{10}$$

where z is the vertical distance from the plane. On the bump and the surrounding plane, the full solution will satisfy

$$\phi^{(1)}=\phi^{(0)}+\phi^{(1)\prime}=0 \tag{11}$$

and should merge with the far-field solution,

$$\phi^{(1)\prime}\to 0 \ , \quad z\to\infty \ . \tag{12}$$

In order to obtain $\phi^{(1)\prime}$, a regular perturbation procedure is followed. The general solution of Laplace's equation can be expressed as a linear combination of the decaying solid spherical harmonics. We obtain the dipole solution for the perturbation

$$\phi^{(1)\prime}=-a_1^3\frac{\nabla\phi^{(0)}\cdot\mathbf{x}}{|\mathbf{x}|^3}=-a_1^3\Lambda\frac{z}{|\mathbf{x}|^3} \ . \tag{13}$$

We make the sparse distribution assumption ($\rho\ll 1$) to neglect the effect of the *same* generation bumps on each other. The total flux due to the perturbation is

$$\int_U \nabla\phi^{(1)\prime}\cdot\mathbf{n}\,dA \ , \tag{14}$$

where U is either the bump B or the surrounding plane P (P denotes the entire plane minus the base of the bump). Over the hemisphere B,

$$\mathbf{n}=\frac{\mathbf{x}}{|\mathbf{x}|} \ , \quad \text{hence } \nabla\phi^{(1)\prime}\cdot\mathbf{n}=2\frac{\Lambda z}{a_1} \tag{15}$$

and, over the surrounding plane,

$$\mathbf{n}=\mathbf{k}, \quad \nabla\phi^{(1)\prime}\cdot\mathbf{n}=-\frac{\Lambda a_1^3}{|\mathbf{x}|^3} \ , \tag{16}$$

where $\mathbf{k}$ is the unit vector in the vertical direction. The integrations over B and P reduce, respectively, to

$$2\pi\frac{\Lambda}{a_1}\int_0^{\pi/2}(a_1\cos\theta)a_1^2\cos\theta\,d\theta=2\pi a_1^2\Lambda \tag{17}$$

and

$$2\pi a_1^3\Lambda\int_{a_1}^{\infty}\frac{1}{r^3}r\,dr=-2\pi a_1^2\Lambda \ , \tag{18}$$

where r and θ are spherical polar coordinates. It should be noted that the upper limit for the P integration is extended to $r\to\infty$ also for the higher generation bumps B's even when they are on top of larger bumps. Strictly this approximation is justified only in the limit $b\to 0$. So the perturbation creates an equal and opposite flux from the bump and the surrounding plane. This indicates that the total flux is a conserved measure.

It should be noted that the measurement of the bumps' area in the previous section assumes $b\ll 1$. It also enables us to treat the field around an i-bump sitting on a j-bump ($i>j$) locally as i-bump sitting on a plane of infinite radius of curvature ($a_i/a_j\to\infty$).

We place 2-bumps on the next stage of the generation. By the above discussion, the perturbation due to a 2-bump, $\phi^{(2)\prime}(\mathbf{x})$, is also a dipole with strength proportional to the local flux density $\mathbf{n}(\mathbf{x})\cdot\nabla\phi^{(1)}(\mathbf{x})$ at $\mathbf{x}$ due to the first generation solution. But the local flux density is not a constant as it is in the case of the starting flat surface. From expressions (15) and (16), we get on the bump,

$$\mathbf{n}(\mathbf{x})\cdot\nabla\phi^{(1)}(\mathbf{x})=3\Lambda\cos\theta \ , \quad \cos\theta=\frac{z}{a_1} \ , \tag{19}$$

and over the plane,

$$\mathbf{n}(\mathbf{x})\cdot\nabla\phi^{(1)}(\mathbf{x})=\Lambda\left[1-\frac{1}{s^3}\right] \ , \quad s=\frac{|x|}{a_1} \ . \tag{20}$$

The effect of other bumps can be shown to be of order $\rho^{3/2}$. Next one needs to establish the probability that a 2-bump will be placed at a certain angle θ or radial distance s. The starting point is the basic assumption that bumps are placed with uniform probability over the entire available surface. This has to be related to the probability density for the perturbation $\phi^{(2)\prime}(\mathbf{x})$. In order to proceed, we divide the available area into three zones: (a) a bump of radius a_1, (b) an annular disk of width $(\lambda-1)a_1$ surrounding a bump, and (c) the rest of the plane (see Fig. 2). The motivation for this artificial division of the plane is the underlying perturbative nature of the solution (allowed by the dilute number density of small bumps) implying that the spatial variation in the flux density as we go further away from a bump becomes negligible. Since region (c) is a complicated shape, it appears difficult to express the local flux as a function of some spatial parameter. Therefore we account for the flux variability with s on the annular disk of arbitrary width but prescribe a constant flux in region (c). Since the width parameter λ of the disk is arbitrary, we will examine the effect of different widths on our analysis ($\lambda=1$ corresponds to no annular disk, i.e., one approximates the flux over the entire plane as a constant). In regions (a) and (b), we take into account the variation of the flux with the appropriate probability density functions. For

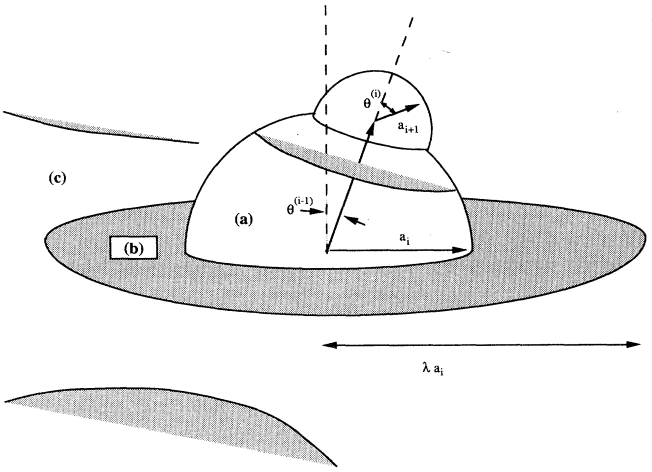

FIG. 2. Sketch of the three different regions used to compute the flux at two levels of the construction process: Region (a) is the hemispherical bump, (b) is the (shaded) disk of outer radius λa_i surrounding every bump, and (c) is the buffer region that fills the space between the disks of different bumps.

(c), we assume a point mass in the probability measure of magnitude sufficient to preserve the conservative nature of the total flux. As evident from the previous section, area fractions on the bump, the disk, and the plane are

$$2\rho, \quad (\lambda^2-1)\rho, \quad 1-\lambda^2\rho, \tag{21}$$

respectively. Hence the probabilities of different regions are

$$\frac{2\rho}{1+\rho}, \quad \frac{(\lambda^2-1)\rho}{1+\rho}, \quad \frac{1-\lambda^2\rho}{1+\rho}. \tag{22}$$

Using these as appropriate partial normalizations, the flux densities or equivalently the dipole strengths for the perturbation [see (19) and (20)] and their corresponding probability densities are the following: In region (a)

$$\Lambda_1^a=\Lambda 3\cos\theta=\Lambda M^a(\theta) \quad \text{with PDF } p(\theta)=\frac{2\rho}{1+\rho}\sin\theta, \tag{23}$$

in region (b)

$$\Lambda_1^b=\Lambda\left[1-\frac{1}{s^3}\right]=\Lambda M^b(s) \quad \text{with PDF } p(s)=\frac{2\rho}{1+\rho}s, \tag{24}$$

and in region (c)

$$\Lambda_1^c=\Lambda\frac{1-\lambda^2\rho-2\rho/\lambda}{1-\lambda^2\rho}=\Lambda M^c \quad \text{with PDF } p(m)=\frac{1-\lambda^2\rho}{1+\rho}\delta(m-M^{(c)}), \tag{25}$$

where $\theta\in[0,\pi/2]$ and $s\in[1,\lambda]$. The probability densities are normalized so that they yield the expressions (22) after integrating over the appropriate ranges of the random variables θ, s, and m.

After placing 3-bumps on the second generation surface, to calculate $\phi^{(3)\prime}$, we will continue in the same way, i.e., divide the available area in three regions locally near a 2-bump. In the scaled variables henceforth denoted by superscript (1) the corresponding strengths and their probabilities can be obtained. We will denote the different types of sites symbolically by a combination of superscripts a, b, and c, i.e., 2-bumps on 1-bumps, 2-bumps on annular disks of 1-bumps, and 2-bumps on the plane region are denoted by Λ_2^{aa}, Λ_2^{ab}, Λ_2^{ac}; annular disks of 2-bumps on 1-bumps, on annular disks of 1-bumps, and on plane by Λ_2^{ba}, Λ_2^{bb}, Λ_2^{bc}; and similarly for the rest plane of 2-bumps on 1-bumps, on disks of 1-bumps, and on plane by Λ_2^{ca}, Λ_2^{cb}, Λ_2^{cc}. For all these different sites the flux densities and their probabilities are

$$\begin{aligned}
&\Lambda_2^{aa}=\Lambda M^a(\theta^{(1)})M^a(\theta) && \text{with joint PDf } p(\theta^{(1)},\theta)=p(\theta^{(1)})p(\theta),\\
&\Lambda_2^{ab}=\Lambda M^a(\theta^{(1)})M^b(s) && \cdots \quad p(\theta^{(1)},s)=p(\theta^{(1)})p(s),\\
&\Lambda_2^{ac}=\Lambda M^a(\theta^{(1)})M^c && \cdots \quad p(\theta^{(1)},m)=p(\theta^{(1)})p(m),\\
&\Lambda_2^{ba}=\Lambda M^b(s^{(1)})M^a(\theta) && \cdots \quad p(s^{(1)},\theta)=p(s^{(1)})p(\theta),\\
&\Lambda_2^{bb}=\Lambda M^b(s^{(1)})M^b(s) && \cdots \quad p(s^{(1)},s)=p(s^{(1)})p(s),\\
&\Lambda_2^{bc}=\Lambda M^b(s^{(1)})M^c && \cdots \quad p(s^{(1)},m)=p(s^{(1)})p(m),\\
&\Lambda_2^{ca}=\Lambda M^c M^a(\theta) && \cdots \quad p(m,\theta)=p(m)p(\theta),\\
&\Lambda_2^{cb}=\Lambda M^c M^b(s) && \cdots \quad p(m,s)=p(m)p(s),\\
&\Lambda_2^{cc}=\Lambda M^c M^c && \cdots \quad p(m,m)=p(m)p(m).
\end{aligned}$$

This is a random multiplicative process as we proceed towards higher generations of the surface. At every level the different strengths of the perturbative dipole solutions are attained by multipliers which are random variables occurring with a prescribed probability density function. After n iterations, the flux density at a site characterized by n variables can be written as

$$\Lambda_n(\ldots\theta^{(r)}\ldots s^{(j)}\ldots m\ldots\theta^{(k)}\ldots)=\prod_{i=1}^{n}M_{(i)}\Lambda \tag{26}$$

with appropriate joint probability density of the n variables. $M_{(i)}$'s are the multipliers [to be drawn either from the set $M(\theta)$, $M(s)$, or M^c] at the ith stage of the flux density calculation or the $(i+1)$th stage of strength of the perturbative dipole computation.

At this stage, we reiterate the various approximations that have been made. (i) The bumps of same generations do not affect each other which is justified by their being well separated (i.e., ρ being small). (ii) Successive generations of bumps have vanishing ratio of their radii, $b\to 0$,

which allows for the neglect of the effect of the finite radius of curvature of the bump beneath, and a bump is treated as though it is placed on a plane. It is to be noted that in the numerical solution for Laplace's equation around a deterministic Koch curve, Everstz and Mandelbrot [18] found that "the larger-scale features of the potential field, as defined by a certain level of the geometric cascade, are virtually left untouched by the additional geometric details added by the next step of the cascade." It would thus appear that the approximations used in the present study are warranted.

V. MULTIFRACTAL STATISTICS

Let us approximate the fractal boundary with small area elements (tiles) U_i, $i=1,2,\ldots$, whose (linear) size is one order smaller than the smallest bump (linear extent $a_{n+1}=a_0 b^{n+1}$). We define the μ_i as the total flux in such an element

$$\mu_i=\int_{U_i}\nabla\phi\cdot\mathbf{n}\,dA\sim a_{n+1}^2\Lambda_n \ . \tag{27}$$

The findings of the previous section imply that this quantity (a random variable) exhibits fluctuations whose statistics depends on n. In order to cast these flux statistics in a framework that exhibits most easily its underlying self-similarity, we use the multifractal formalism. We focus on the average of the qth-order "moment" $\langle\sum_i\mu_i^q\rangle$ where μ_i is the total flux in such an element of size a_{n+1}, and the sum is extended over all elements. The desired quantity can be obtained as

$$\left\langle\sum_i\mu_i^q\right\rangle\sim\Lambda^q a_{n+1}^{2q}\left\langle\sum_i\prod_{j=1}^{n}M_{(j)}^q\right\rangle=\Lambda^q a_{n+1}^{2q}N\left\langle\prod_{j=1}^{n}M_{(j)}^q\right\rangle \ , \tag{28}$$

where N is the total number of elements,

$$N\sim\frac{(1+\rho)^n S}{a_{n+1}^2} \ . \tag{29}$$

As is evident from the previous section, the probabilities of multipliers on regions of different generations are independent because bumps are placed with the same density per unit area on bumps, disks, or buffer regions. Thus the joint probabilities reduce to products of the individual probabilities. Hence we obtain

$$\left\langle\prod_{j=1}^{n}M_{(j)}^q\right\rangle=\langle M^q\rangle^n \ . \tag{30}$$

The q moment of the random variable M can be obtained by appropriately integrating over its possible values, as

$$\begin{aligned}\langle M^q\rangle&=\int_0^{\pi/2}(3\cos\theta)^q\frac{2\rho}{1+\rho}\sin\theta d\theta+\int_0^{\lambda}\left[1-\frac{1}{s^3}\right]^q\frac{2\rho}{1+\rho}s\,ds+\left[\frac{(1-\lambda^2\rho-2\rho/\lambda)}{1-\lambda^2\rho}\right]^q\frac{1-\lambda^2\rho}{1+\rho}\\&=\frac{2\rho}{1+\rho}\left[\frac{3^q}{1+q}+I(q,\lambda)\right]+\left[\frac{1-\lambda^2\rho-2\rho/\lambda}{1-\lambda^2\rho}\right]^q\frac{1-\lambda^2\rho}{1+\rho} \ ,\end{aligned} \tag{31}$$

where

$$I(q,\lambda)=\int_0^{\lambda}\left[1-\frac{1}{s^3}\right]^q s\,ds \ . \tag{32}$$

Writing this in terms of the usual multifractal moment exponents [19] $\tau(q)$ we obtain (in the limit of large n)

$$\left\langle\sum_i\mu_i^q\right\rangle\sim\Lambda^q S a_0^{2q-2}\left[\frac{a_{n+1}}{a_0}\right]^{\tau(q)} \ , \tag{33}$$

where

$$\tau(q)=2(q-1)+\log_b\left[2\rho\left[\frac{3^q}{1+q}+I(q,\lambda)\right]+\left[1-\lambda^2\rho-\frac{2\rho}{\lambda}\right]^q(1-\lambda^2\rho)^{1-q}\right] \ . \tag{34}$$

For $q=0$, we retrieve the fractal dimension of the surface $\tau(0)=-D$. For $q=1$ one obtains $\tau(1)=0$, meaning that the sum of the flux over all area elements is a constant independent of n (conservative measure). Since the values of the multipliers M are accurate up to $O(\rho^{3/2})$, $\tau(q)$ obtained in Eq. (34) can be shown to be accurate up to $O(q\rho^{3/2}/\ln b)$, which is small.

The corresponding singularity distribution function $f(\alpha)$ for Holder exponents [20] α is obtained through the Legendre transform

$$f(\alpha(q))=q\alpha(q)-\tau(q) \ , \tag{35}$$

$$\alpha(q)=\frac{d\tau}{dq}=2+\frac{F_1+F_2}{F_3\log_e b} \ , \tag{36}$$

where

$$F_1=2\rho\left[\frac{3^q}{1+q}\log_e 3-\frac{3^q}{(1+q)^2}+\frac{\partial I}{\partial q}\right],$$
$$F_2=\left[1-\lambda^2\rho-\frac{2\rho}{\lambda}\right]^q(1-\lambda^2\rho)^{1-q}\log_e\left[\frac{1-\lambda^2\rho-2\rho/\lambda}{1-\lambda^2\rho}\right], \quad (37)$$
$$F_3=2\rho\left[\frac{3^q}{1+q}+I(q,\lambda)\right]+\left[1-\lambda^2\rho-\frac{2\rho}{\lambda}\right]^q(1-\lambda^2\rho)^{1-q}.$$

We note that for the above treatment to be meaningful, we need to restrict ρ so that the flux density in the rest of the plane remain positive. The desired restriction is

$$1-\lambda^2\rho-\frac{2\rho}{\lambda}>0 \quad \text{or} \quad \rho=\frac{1}{b^{D-2}}-1<\frac{1}{(\lambda^2+2/\lambda)}. \quad (38)$$

It depends on λ, the width of the annular disk in the units of the radius of the bumps. Evidently the area fraction ρ becomes more and more constrained as we increase the disk width. Furthermore, the q values are to be limited to the range $-1<q<\infty$, because for $q\le -1$, α is not defined [the integral $I(q,\lambda)$ and $3^q/(1+q)$ diverge]. This is because of the fact that on the circle where the bumps intersect the plane, the flux density is locally zero. This is emphasized by the negative moments. We will return to a more detailed discussion of this point at a later stage. The results to be presented will thus be restricted to the range from $q>-0.5$ up to $q=20$.

The value of λ is arbitrary; it is not a physical parameter but only one used for the calculation. To justify this approach, the results should be reasonably independent of the precise λ value chosen. We thus perform a λ-sensitivity test of the $f(\alpha)$ curve, for a dimension $D=2.15$ and $b=0.33$ (Fig. 3). Only a negligible dependence on λ is observed. This means that the variability of the flux on the plane is not important as far as the left side of $f(\alpha)$ is concerned. In other words, averaging the flux on the buffer region of the plane and having a lumped mass in the probability distribution is quite justified in the limit of a dilute distribution of the bumps.

Next, the dependence of $f(\alpha)$ on the geometric parameters of the problem, ρ and b, is explored. Evidently, it depends on both the parameters. Even if we fix the fractal dimension D, different pairs of ρ,b lead to different flux statistics. We exemplify this by fixing $D=2.15$. Figure 4 shows different $f(\alpha)$'s all peaking at 2.15. As b is increased (and ρ is decreased) the left side of the curves become steeper and the limiting value of $f(\alpha_{\min})$ becomes smaller.

We can inquire in more detail about the left limit of the distribution, given by $\alpha_{\min}$. This is the strongest singularity which will occur if bumps of all sizes are placed precisely on top of their predecessor bump ($\theta^{(i)}=0$ for all i). This is of course very unlikely to occur [its $f(\alpha)\ll 0$]. In this case the multiplier at each stage takes on its largest value, $M=3$, and the measure in an area element of size a_n will thus be $\mu_{\max}=3^n a_n^2$. By the definition of α this corresponds to

$$\alpha_{\min}=\frac{\ln(\mu_{\max})}{\ln(a_n/a_0)}=2+\log_b 3. \quad (39)$$

This is indeed consistent with the limits in Fig. 4.

Expressions have been found that condense considerable statistical information about the locally integrated flux μ. This can be illustrated by recalling (Mandelbrot [21]) that the function $f(\alpha)$ is related to the probability density distribution $P(\mu)$ of the measure as follows. Locally the random variable μ can be expressed in terms of the new random variable

$$\alpha'=\frac{\ln(\mu)}{\ln(r/a_0)}. \quad (40)$$

Then, the probability of picking a segment V_i of linear

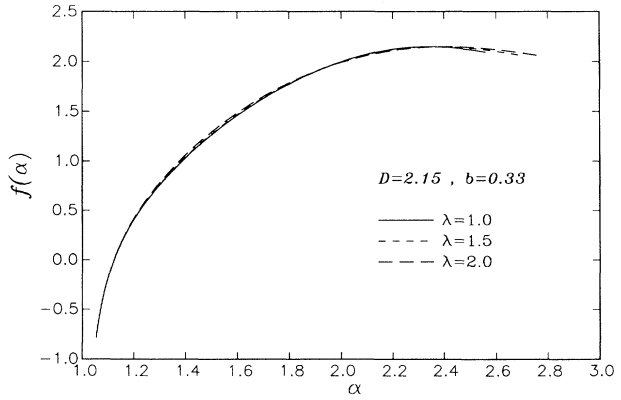

FIG. 3. $f(\alpha)$ for $D=2.15$ and $b=0.33$ and various λ's, evaluated for $-0.5<q<20$.

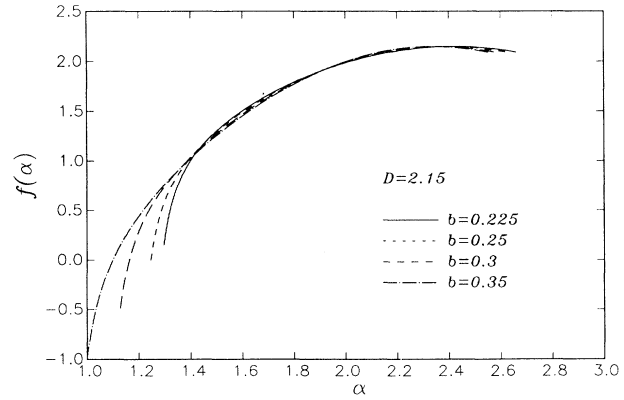

FIG. 4. $f(\alpha)$ for surfaces corresponding to $D=2.15$ but varying b, for $-0.5<q<20$.

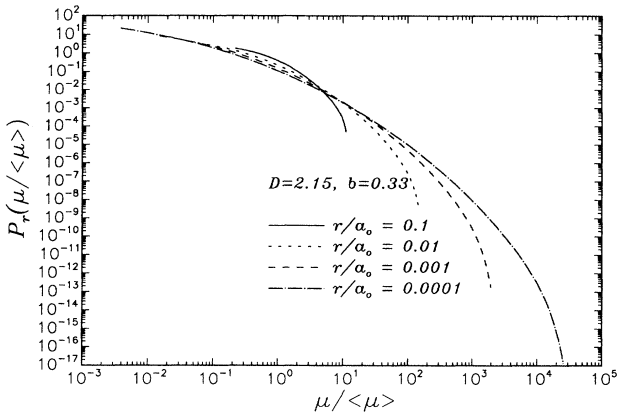

FIG. 5. Probability density $P_r(\mu)$ of the flux μ, around a fractal surface with $D=2.15$, and $b=0.33$, corresponding to different scales r.

extent r, where α' takes on a value between α and $\alpha+d\alpha$ is of the order of

$$P_r(\alpha)d\alpha \sim \left[\frac{r}{a_0}\right]^{D-f(\alpha)} d\alpha \ . \tag{41}$$

It follows that the probability density distribution for μ is given by

$$P_r(\mu)=c\left[\frac{r}{a_0}\right]^{D-f(\ln(\mu)/\ln(r/a_0))} \frac{1}{\mu \ln(r/a_0)} \ , \tag{42}$$

where c is a constant of normalization. As an example, we consider $D=2.15$ and $b=0.33$. Figure 5 shows $P_r(\mu/\langle\mu\rangle)$ as a function of $\mu/\langle\mu\rangle$ for different values of the scale r. It is clear that the variability of μ (relative to its mean value $\langle\mu\rangle$) greatly increases for decreasing scales r. Because of the restriction $q>-1$ used to obtain $f(\alpha)$ we cannot compute $P_r(\mu/\langle\mu\rangle)$ over its entire range, but only from its peak to the high μ values.

In the next section we explore the consequences of an additional approximation; namely, that of averaging, at every step, the flux density over the bumps.

VI. BINOMIAL APPROXIMATION

In the previous section, we took into account the variability of the flux density on the bumps and on the surrounding plane by endowing the successive multipliers with a probability density function depending on location. It was further established that the resulting statistics are not very sensitive to the variation of the disk width, parametrized by λ. In fact $\lambda=1$ corresponds to assigning an average value for the flux density on the entire plane. In this section, the effect of assigning an average flux density for the bumps also is examined. There is a further motivation for this averaging procedure. As was noted, the zero flux density at the base circles of the bumps restricts the order of the moments to $q>-1$, giving rise to left-sided singularity distributions. With the average flux density being obtained by two constant multipliers on the bumps and on the plane, the above restriction can be removed. Because of its binomial nature, it closely follows the statistics of the area characterization and a similar symbolic representation is used.

From expressions (17) and (18), the total flux through the bump is $\Lambda S c_1(\pi a_1^2+2\pi a_1^2)=3\Lambda S\rho$. Noting the areas (3), the average flux densities through the 1-bumps $\{1\}$ and the plane $\{0\}$ are

$$\frac{3}{2}\Lambda \ , \quad \frac{1-3\rho}{1-\rho}\Lambda \ , \tag{43}$$

respectively. We observe that the restriction $3\rho<1$ is to be satisfied in view of the above result.

As far as the dipole strength needed for the calculation of $\phi^{(2)\prime}(x)$ is concerned, instead of using the local value at $\mathbf{x}$, $\mathbf{n}(\mathbf{x})\cdot\nabla\phi^{(1)}(\mathbf{x})$, the flux density is replaced by the average flux density over the entire site type. The expression for $\phi^{(2)\prime}$ is therefore

$$\phi^{(2)\prime}=-a_2^3\Lambda_{\text{eff}}^1\frac{z^{(1)}}{r^{(1)^3}} \ , \tag{44}$$

where Λ_{eff}^1's are given by (43). The total contribution due to the perturbations is found using the same analysis as before. Then, for the second generation prefractal surface, we obtain the following average flux densities for sites $\{11\}$, $\{01\}$, $\{10\}$, and $\{00\}$

$$\frac{3^2}{2^2}\Lambda \ , \frac{3}{2}\frac{(1-3\rho)}{(1-\rho)}\Lambda \ , \quad \frac{(1-3\rho)}{(1-\rho)}\frac{3}{2}\Lambda \ , \quad \frac{(1-3\rho)^2}{(1-\rho)^2}\Lambda \ . \tag{45}$$

The above process is repeated and after n stages, statistics for average flux densities are found that are quite similar to the surface statistics:

Binary representation	Flux density	Number
$\{1111\ldots n$ 1's$\}$	$\Lambda(\frac{3}{2})^n$	${}^nC_0$
...	...	...
$\{01101\ldots k$ 1's,$(n-k)$0's$\}$	$\Lambda(\frac{3}{2})^k\left[\frac{1-3\rho}{1-\rho}\right]^{n-k}$	${}^nC_k$
...	...	...
$\{0000\ldots n$ 0's$\}$	$\Lambda\left[\frac{1-3\rho}{1-\rho}\right]^n$	${}^nC_n$

For a generic site the total flux from all sites of that type is the average flux density multiplied by its area viz.

$$\Lambda\left[\frac{3}{2}\right]^k\left[\frac{1-3\rho}{1-\rho}\right]^{n-k} S(2\rho)^k(1-\rho)^{n-k} = \Lambda S(3\rho)^k(1-3\rho)^{n-k} . \quad (46)$$

The total flux is therefore

$$F=\Lambda S\sum_{k=0}^{n} {}^nC_k(3\rho)^k(1-3\rho)^{n-k}=\Lambda S . \quad (47)$$

Again the flux is seen to form a conservative measure since the total flux is a constant, independent of n.

We now cast the above flux statistics into the binomial multifractal formalism. In order to calculate $\sum_i \mu_i^q$, with the resolution of the scale of size a_n, we note that there will be A_p/a_n^2 elements where the flux is $\Lambda_p a_n^2$, where A_p and Λ_p are the area and average flux density of the sites for the pth permutation. Then the summation can be performed over all different sites corresponding to the pth permutations of the n-digit binary numbers according to

$$\sum_i \mu_i^q=\sum_p \frac{A_p}{a_n^2}(\Lambda_p a_n^2)^q . \quad (48)$$

Substitution of different expressions, and a binomial summation reduces (48) to

$$\sum_i \mu_i^q=a_0^{2q-2}\Lambda^q S\{b^{2q-2}[(3\rho)^q(2\rho)^{1-q}+(1-3\rho)^q(1-\rho)^{1-q}]\}^n , \quad (49)$$

which can be written as

$$\sum_i \mu_i^q=\Lambda^q S a_0^{2q-2}\left[\frac{a_n}{a_0}\right]^{\tau(q)} , \quad (50)$$

where

$$\tau(q)=2(q-1)+\log_b[(3\rho)^q(2\rho)^{1-q}+(1-3\rho)^q(1-\rho)^{1-q}] . \quad (51)$$

For $q=0$, we again retrieve the fractal dimension of the surface $\tau(0)=-D$, while $\tau(1)=0$, as required by the conservative nature of the process. The singularity distribution and the expression for α are

$$f(\alpha(q))=q\alpha(q)-\tau(q) , \quad (52)$$

$$\alpha(q)=\frac{d\tau}{dq}=2+\frac{(3\rho)^q(2\rho)^{1-q}\log_b\left[\frac{3\rho}{2\rho}\right]+(1-3\rho)^q(1-\rho)^{1-q}\log_b\left[\frac{1-3\rho}{1-\rho}\right]}{(3\rho)^q(2\rho)^{1-q}+(1-3\rho)^q(1-\rho)^{1-q}} . \quad (53)$$

To explore the dependence of $f(\alpha)$ on the parameters, we take different pairs of ρ and b for $D=2.15$, and Fig. 6 shows the corresponding $f(\alpha)$'s. As before, while b is increased (and ρ is decreased) the left side of the curve becomes steeper and the limiting value of $f(\alpha_{\min})$ becomes smaller. We see that the right side of $f(\alpha)$ curves achieves its limiting value quite soon.

We obtain the values of the limits of the distribution by taking the limits of Eq. (53) for large q using $3(1-\rho)/2(1-3\rho)>1$,

$$\alpha_{\min}\equiv\lim_{q\to\infty}\alpha(q)=2+\log_b(\tfrac{3}{2}) \quad (54)$$

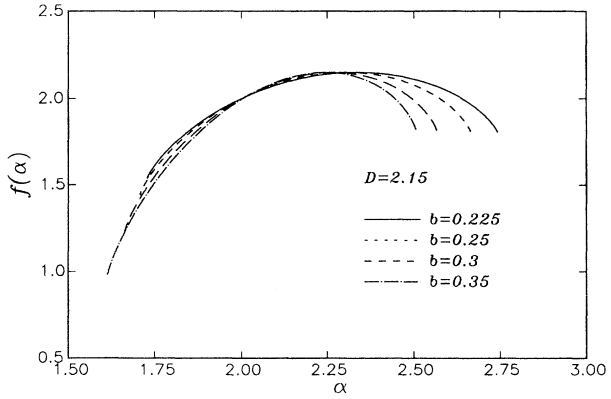

FIG. 6. $f(\alpha)$ for surfaces corresponding to $D=2.15$ but varying b for the binomial approximation.

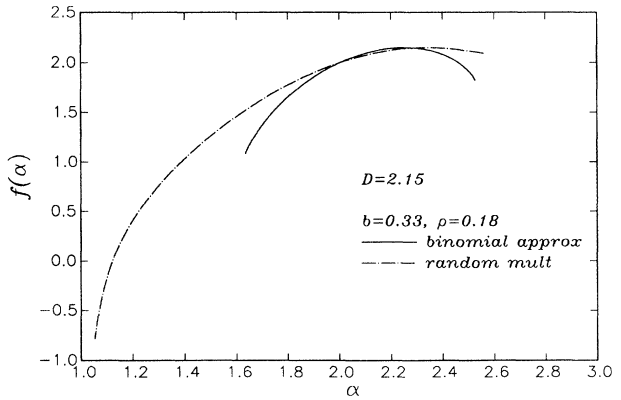

FIG. 7. Comparison of $f(\alpha)$ for binomial approximation and random multiplier approach ($D=2.15$, $b=0.33$).

and

$$\alpha_{\max} \equiv \lim_{q \to -\infty} \alpha(q) = 2 + \log_b \left[\frac{1-3\rho}{1-\rho} \right] . \quad (55)$$

Finally, this is now compared with the results of the random multiplier approach of the previous section. For both, $f(\alpha)$ is calculated using $b=0.33$ and $\rho=0.18$ (i.e., $D=2.15$), and is shown in Fig. 7. We see that the two approaches yield significantly different results. Only in the neighborhood of the peak do they agree to some extent. Comparing Eqs. (39) and (54) shows that the minimum α values differ by $\log_b 2$, which is significant. This shows that averaging the flux over the bump at every step does not yield the correct $f(\alpha)$ spectrum.

VII. SUMMARY AND DISCUSSION

A perturbative approach has been used to obtain analytic expressions for the statistical properties of the gradient of potential fields on a fractal surface. This surface is composed of semihemispherical bumps of increasingly smaller sizes placed randomly over an initially smooth plane. The approximations used to solve the problem are valid at small "roughness," characterized by a surface dimension $D=2+\epsilon$, with small ϵ. The limitations of the present study, namely, the sparse distribution assumption as well as the large scale ratio between consecutive stages, were necessary in order to treat the problem analytically. Using a random multiplier approach, the left side of $f(\alpha)$ was determined. The resulting expressions for $f(\alpha)$ were shown to depend not only on D but also on other parameters characterizing the surface geometry. In general then, we point out that characterizing a rough surface using its fractal dimension only is insufficient to treat the harmonic problem. We illustrated the implications of these findings on the flux statistics by explicitly showing probability distribution functions for different resolutions, or cutoffs. However, a stronger binomial approximation of the multiplicative process was shown to yield results that differ considerably from those of the complete statistical treatment of flux multipliers. This illustrates possible dangers of averaging multiplier statistics before their product is taken.

In terms of the relevance of these findings on the actual potential field $\phi(\mathbf{x})$ surrounding the fractal boundary, we now make some qualitative observations: If we inquire about the value of the potential field ϕ at a distance r from the boundary, we argue that it is of the order of the average normal gradient over a region of area r^2, multiplied by the distance r. We can distinguish between three regimes as follows.

If $r \gg a_0$, then $\phi \sim r\Lambda$ because the convolutions of the boundary are not felt at this distance. If we look at points very close to the boundary at distances smaller than a_n (the size of the smallest bumps on the surface), i.e., $r \ll a_n$, then ϕ becomes a random variable. It is related to the measure μ by $\phi \sim r(\mu/a_n^2)$, where μ is the flux occurring in segments of the boundary of size a_n and whose statistical distribution is given by $P_{a_n}(\mu)$. If we consider points at an intermediate distance from the boundary $a_n < r < a_0$, then $\phi \sim r(\mu/r^2)$, where μ is the coarse-grained flux at resolution r. Its statistics are thus given by $P_r(\mu)$.

Far from the boundary the multifractal nature of the gradient is more or less irrelevant for the field statistics. Close to the boundary ($a_n < r < a_0$) the mean flux, and the mean field, are again relatively unaffected by the fractal boundary because of the requirement of conservation (yielding a scale-independent mean). However, using the above plausibility arguments relating the field at some distance r to the coarse-grained flux on the boundary, the field will locally go like $\phi \sim r^{(\alpha-1)}$ [with probability density $P_r(\alpha)$]. The fastest decay away from the boundary will be observed when $\alpha=\alpha_{\min}$ (at the "tips" of the boundary).

In terms of statistics, higher-order moments of the field can be strongly dependent on cutoff, resolution, and distance to the boundary. For instance, $\mathcal{S}$, the skewness of the field, will go like

$$\mathcal{S} \equiv \frac{\langle \phi^3 \rangle}{\langle \phi^2 \rangle^{3/2}} \sim \frac{\langle (\mu/r)^3 \rangle}{\langle (\mu/r)^2 \rangle^{3/2}} \sim r^{\tau(3)-(3/2)\tau(2)-(1/2)D} . \quad (56)$$

For example, in the numerical example considered in Sec. V with $D=2.15$ and $b=0.33$, this yields $\mathcal{S} \sim r^{-1.392}$, i.e., it diverges as $r \to 0$.

Therefore, an *approximate* statistical characterization of the entire potential field parametrized by its distance to the boundary is possible.

ACKNOWLEDGMENTS

Many thanks are due to Professor A. Prosperetti for encouragement and fruitful conversations on this topic. We also thank Professor P. Jones for bringing certain references [15–17] to our attention. K. S. acknowledges the financial support of NSF (Grant No. CBT-891844) and C. M. that of NSF (Grant No. CTS-9113048) and ONR (Grant No. N00014-92-J-1109) on turbulence modeling.

[1] T. A. Witten and L. M. Sanders, Phys. Rev. Lett. **47**, 1400 (1981).
[2] J. Feder, *Fractals* (Plenum, New York, 1988).
[3] L. Pietronero and Wiesmann, J. Stat. Phys. **36**, 909 (1984).
[4] T. Nagatani, J. Phys. A **20**, L381 (1987).
[5] T. Nagatani, J. Phys. A **20**, 6135 (1987).
[6] T. Nagatani, Phys. Rev. A **36**, 5812 (1987).
[7] L. Pietronero, A. Erzan, and C. J. G. Everstz, Phys. Rev. Lett. **61**, 861 (1988).
[8] B. B. Mandelbrot and C. J. G. Everstz, Nature (London) **348**, 143 (1990).
[9] P. Meakin, A. Coniglio, H. E. Stanley, and T. A. Witten, Phys. Rev. A **34**, 3325 (1986).
[10] K. R. Sreenivasan, R. Ramashankar, and C. Meneveau,

Proc. R. Soc. London, Ser. A **421**, 79 (1989).
[11] O. M. Phillips, Proc. Cambridge Philos. Soc. **51**, 220 (1955).
[12] R. W. Stewart, J. Fluid Mech. **1**, 593 (1956).
[13] L. Carleson, Ann. Acad. Sci. Fenn., Ser. A 1 : Math. Phys. **10**, 113 (1985).
[14] N. G. Makarov, Proc. London Math. Soc. **51**, 369 (1985).
[15] N. G. Makarov, *Proceedings of the International Congress of Mathematicians, Berkeley, CA, 1986* (American Mathematical Society, Providence, 1987), p. 766.
[16] P. Jones and T. Wolff, Acta Math. **161**, 131 (1988).
[17] T. Wolff (unpublished).
[18] C. J. G. Everstz and B. B. Mandelbrot, J. Phys. A **25**, 1781 (1992).
[19] H. G. E. Hentschel and I. Procaccia, Physica **8**, 435 (1983).
[20] T. C. Halsey, M. H. Jensen, L. P. Kadanoff, and I. Procaccia, Phys. Rev. A **33**, 1141 (1986).
[21] B. B. Mandelbrot, Pure Appl. Geophys. **131**, 5 (1989).